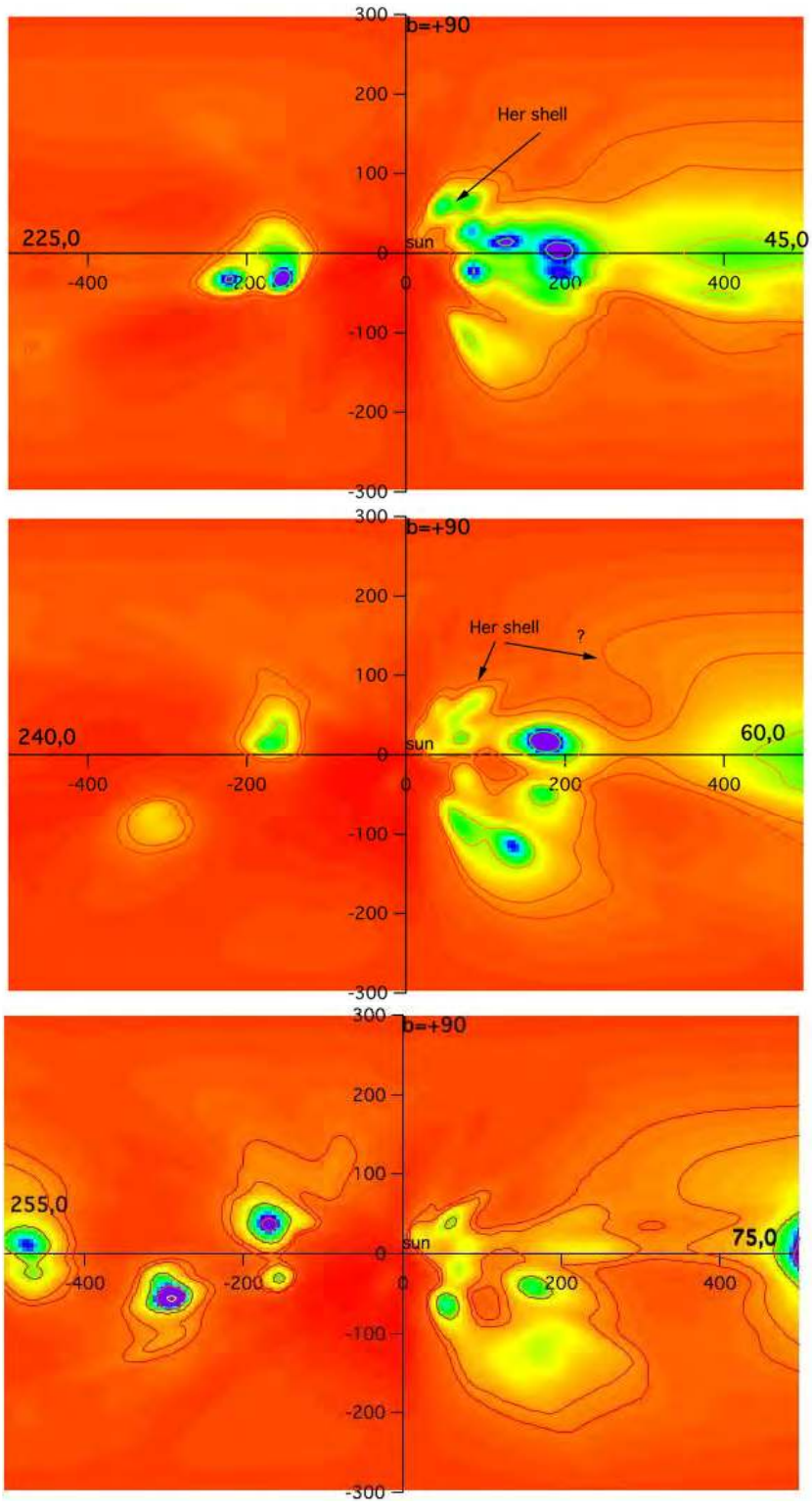

Fig. 5. Same as Fig. 4 for the next three vertical planes. In the $l = 45°$ and $l = 60°$ half planes (*top* and *middle*), the HI Hercules shell is indicated at the 60–150 pc distance derived by Lilienthal et al. (1992) for its low-velocity component. Such a location is in good agreement with the elongated feature at $b \simeq 40°$. The second component at 250 pc may correspond to the fainter distant feature in the $l = 60°$ half plane.

4.2. Extinction in vertical planes

We show in Figs. 4 to 7 the opacity distributions in a series of 12 vertical planes containing the Sun, with two consecutive planes separated by 15° in longitude. For each plane we superimpose – when they happen to be located within 25 pc from it – the locations of the central parts of the nearby OB associations as they have been estimated by de Zeeuw et al. (1999), as well as the HI and CO clouds listed by Perrot & Grenier (2003) and whose distances have been estimated by de Geus et al. (1990), Grenier et al. (1989), Maddalena et al. (1986), Murphy & Myers (1985), Murphy et al. (1986) and Ungerechts & Thaddeus (1987). This allows checking that those structures have their counterpart in the form of a dense region (for the clouds) or a cavity closely bounded by a dense region (for the OB associations) in the inverted maps. We did not include Collinder 121 whose distance has been the object of several discussions (e.g., Kaltcheva & Makarov 2007; Burningham et al. 2003) and maybe

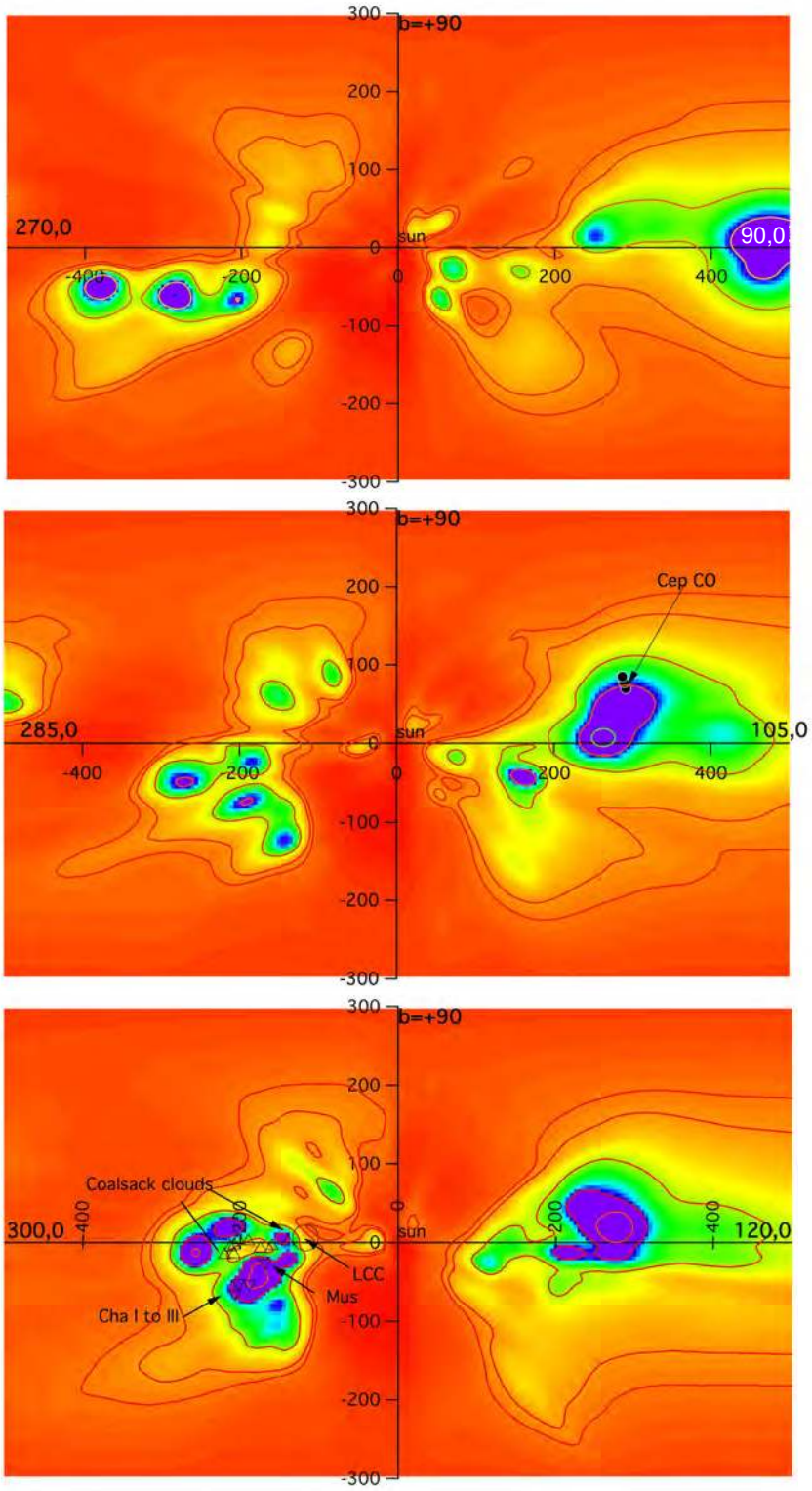

Fig. 6. Same as Fig. 4 for the next three vertical planes.

much larger than 500 pc. The new Hipparcos determinations of van Leeuwen (2007) indeed show that there are various distance ranges for the members. Interestingly, our maps do not reveal any cloud at ≃500 pc in the direction of Col121 (l, b = 236, –10). We also indicate the distances to the main nearby molecular clouds (or cloud complexes) derived by Knude (2010) based on Hipparcos and 2MASS.

One of the main advantages of the present method and of the dataset is the large number of nearby stars for which very low extinctions have been measured. This allows locating nearby tenuous clouds. Indeed, all vertical planes reveal low-density structures above the plane that are isolated or linked to denser structures, and whose shapes do appear quite complex. Because these structures are faint and the target star density decreases with the distance to the plane, they appear blurred sometimes, but the comparison between their locations in the maps and the coordinates of the medium and high-latitude clouds that show up in the 2D dust maps of (Schlegel et al. 1998, hereafter SFD) leaves no doubt about their reality. To allow the reader to make those comparisons we have superimposed on the SFD dust map

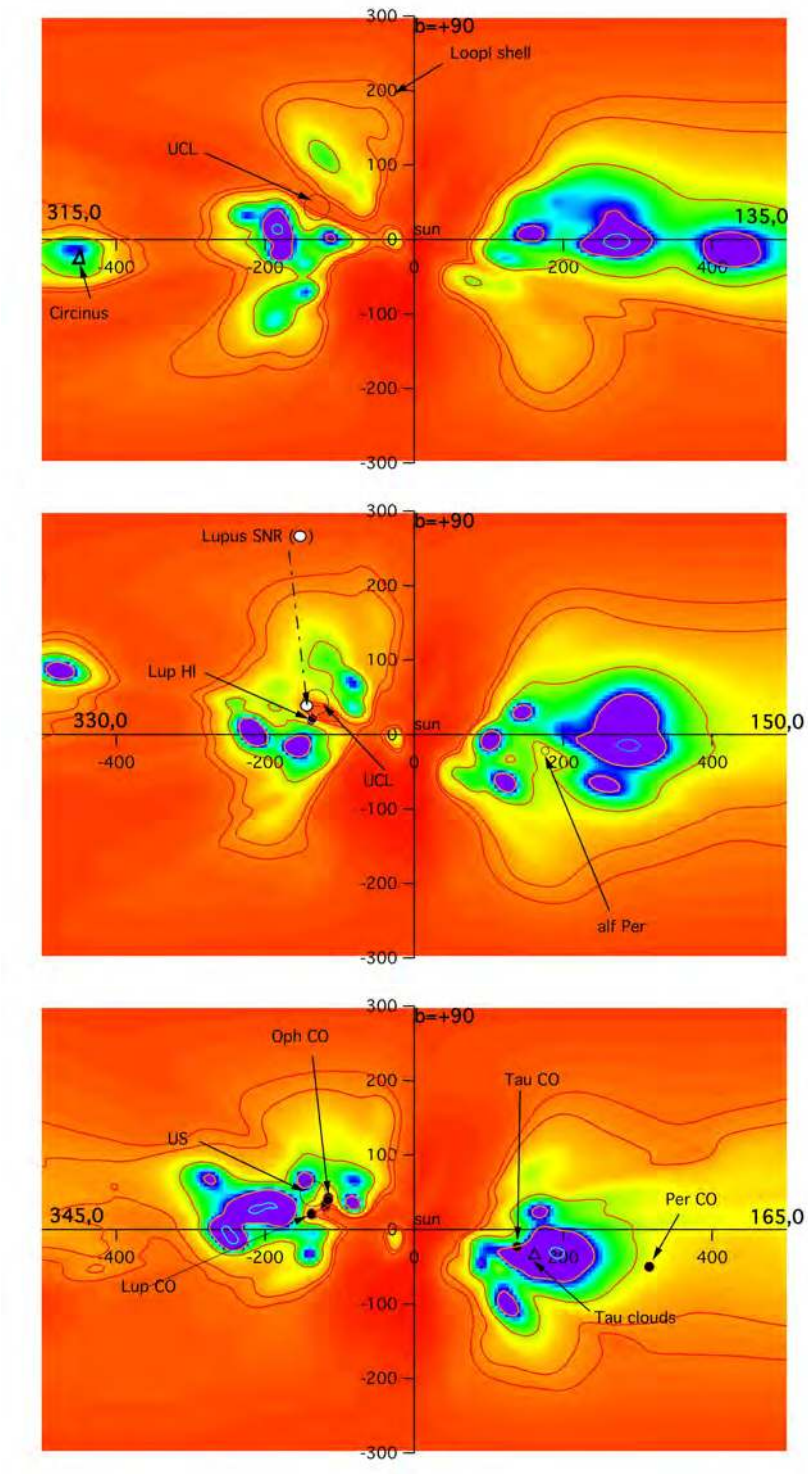

Fig. 7. Same as Fig. 4 for the next three vertical planes.

the traces of the vertical planes of Figs. 4 to 7. This is shown in Fig. 8. We use a logarithmic scale for $E(B-V)$ in order to identify the faint medium and high latitude clouds more easily. Interestingly, almost all features seen in Fig. 8 along those meridian lines have a counterpart under the form of an enhanced opacity in the corresponding vertical plane.

As a first example we consider the $l = 105-285°$ vertical plane (Fig. 6 middle).

i) The $l = 105°$ half plane north: in the SFD map (Fig. 8) there is a northern extension of the dust (yellow contour up to $b = +45°$) and many very small features (seen in yellow) at higher latitudes up to $b = +60$; $+80°$. In Fig. 6 (middle), just above the main concentrations extending from the plane up to $b = +30$; $+40°$ (and colored violet, green, yellow), is a fainter feature apparently linked to the bulk but extending further up to $+45°$ (faint yellow-orange) and located at ≃200 pc. We believe this is the counterpart of the cloud seen in the 2D map. In addition, there is a faint dust cloud located much closer (≤50 pc), that must produce small absorptions up to $+80°$ latitude and probably explains the very faint, high latitude features in the 2D map.
ii) The $l = 285°$ half plane north: in Fig. 8 it can be seen that compared to the previous half plane the opacity is stronger

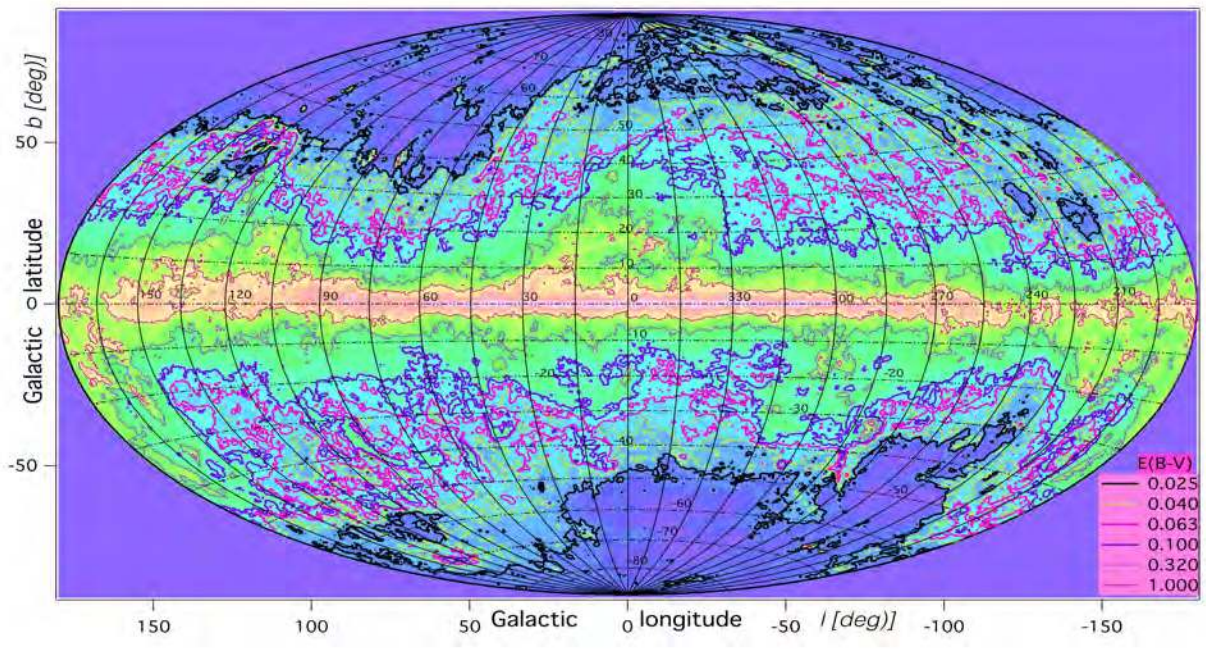

Fig. 8. The Schlegel et al. (1998) dust map is reproduced, along with the traces of the vertical planes of Figs. 4 to 7 superimposed. The color–coded quantity is the logarithm of $E(B-V)$. The six contours are for $\log(E(B-V)) = 0$ (thin pink), –0.5 (thin violet), –1 (thick violet), –1.2 (thick pink), –1.4 (yellow), and –1.6 (black). Counterparts to the tenuous clouds at mid or high latitudes that appear in this SFD map can be searched for in Figs. 4 to 7, using the l, b grid.

at high latitude. More quantitatively, the $E(B-V) = 0.063$ (thick pink) contour extends up to $b = +35°$, instead of +20°. The $E(B-V) = 0.04$ (yellow) contour extends up to +55°, disappears above, then a more opaque area reappears at $b = +55°$. A look at Fig. 6 (middle) indeed shows nearby dust (green) up to $b \simeq +55°$ and faint extensions visible almost up to the pole.

iii) The $l = 105°$ half plane south: in Fig. 8 the $E(B-V) = 0.063$ (thick pink) contour extends down to $b = -55°$, which corresponds to the cloud seen at ≃170 pc in Fig. 6 (pale green and yellow). On the other hand, the 80 pc distant feature at lower latitude ($b = -65°$) in Fig. 6 may be the counterpart to the $b = -70°$ small cloud seen in Fig. 8.

iv) The $l = 285°$ half plane south: in Fig. 8 the $E(B-V) = 0.063$ (thick pink) contour extends down to $b = -45$; $-50°$, which corresponds to the cloud seen at 150 pc in Fig. 6 (dark blue, green, yellow). The –60; –50° small extension seen in Fig. 8 has no clear counterpart but may be simply the southern extension of the previous feature (faint yellow). Alternatively, it may be more distant than 350 pc, or missing due to the lack of constraining targets.

Comparing in the same way all half planes shows that most of the high-latitude features in Fig. 8 are found in the maps. As a second example we consider the $l = 15-195°$ vertical plane in Fig. 4 (middle). At $l = 15°$, the inverted map shows clearly in the north dense high-latitude clouds up to $b = +60°$, with a small extension at even higher latitude (around +70°) that is seen up to 150 pc (in the same direction there is also a very faint cloud much closer to the Sun). This is similarly found in Fig. 8 along the northern part of the $l = +15$ meridian. In the south, Fig. 4 (middle) reveals a dense cloud at $b \simeq -25$; $-30°$ and at $d \simeq 150$ pc, whose emission is clearly marked in the Fig. 8 (green color). At $l = 195°$ there is a strong contrast between the northern latitudes, where an appreciable opacity is reached as low as $b \lesssim +20°$ (transition between yellow and orange), and the south where dust extends down to $b = -55$; –60°. The $l = 195°$ meridian in Fig. 8 indeed shows clearly this low-latitude cloud extension (pink contour) while the same level of dust emission does not go beyond +20° in the north. We note, however, a discrepancy between the total absence of opacities detected in the north in the inverted maps above $b \simeq +30°$ (at this latitude there is a small feature at +450 pc) and the SFD map that shows $E(B-V) = 0.04$ up to +42°. This discrepancy seems to exist for the whole interval $l = 180-230°$. This dust may be much more distant than 1 kpc or missing in the maps due the lack of constraining targets. Apart from this region, agreements exist for all directions, and it is possible to assign a distance to the Fig. 8 high-latitude emission features by using the appropriate maps. This suggests that our limitation of $Z = 300$ pc for the target stars had no significant influence on the results.

Given the limited number of faint stars, the mapping performs in some case less well for the very dense structures, in the sense that dense clouds may be underestimated due to the lack of strongly reddened targets, or their densest areas appearing slightly displaced with respect to the actual cloud centers. This is the case for the Orion structures for example in the $l = 210°$ half plane (Fig. 4 bottom) that are centered at $b = -15°$, while the CO clouds are located a few degrees below. Also, their extent is not as wide as in the 2D maps and they do not appear as opaque as the dust maps predict. Such biases due to the target star distribution and the inversion should disappear by increasing the extinction databases.

Several planes are particularly interesting since they contain well-studied regions and in some case the maps shed some light on their distances; for example the $l = 30°$ half plane crosses the Aquila rift (Fig. 4, bottom). We find a cloud complex at low latitude ($b = 5°$) that starts at ≃190 pc and centered at $d \simeq 220$ pc. It corresponds to the Serpens cloud and its recent distance assignment by Knude (2011) (193 pc) and Straižys et al. (2003) (225 pc). We note that there is a second cloud

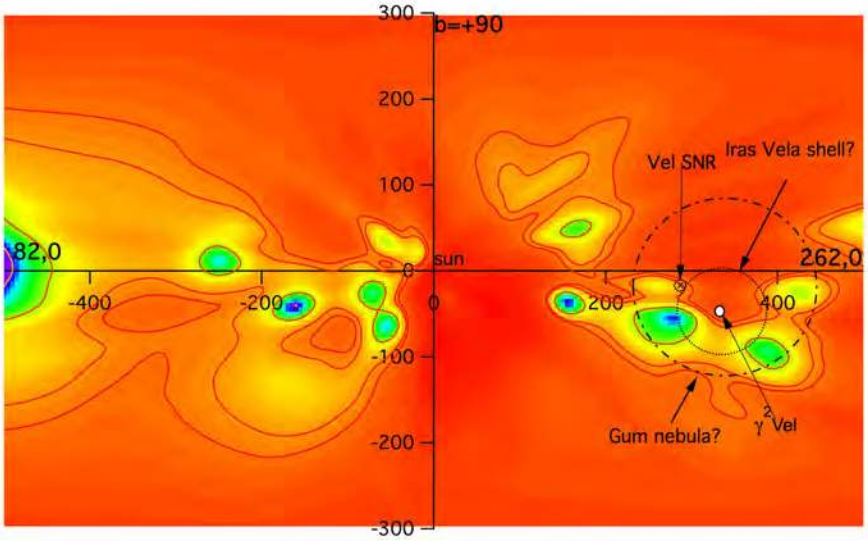

Fig. 9. Same as Fig. 4 for the l = 82–262° plane. The Vela SNR and the Wolf-Rayet system γ_2Vel are shown. The locations of the Iras Vela shell (IVS) and Gum Nebula contours are drawn according to the scenario of Sushch et al. (2011).

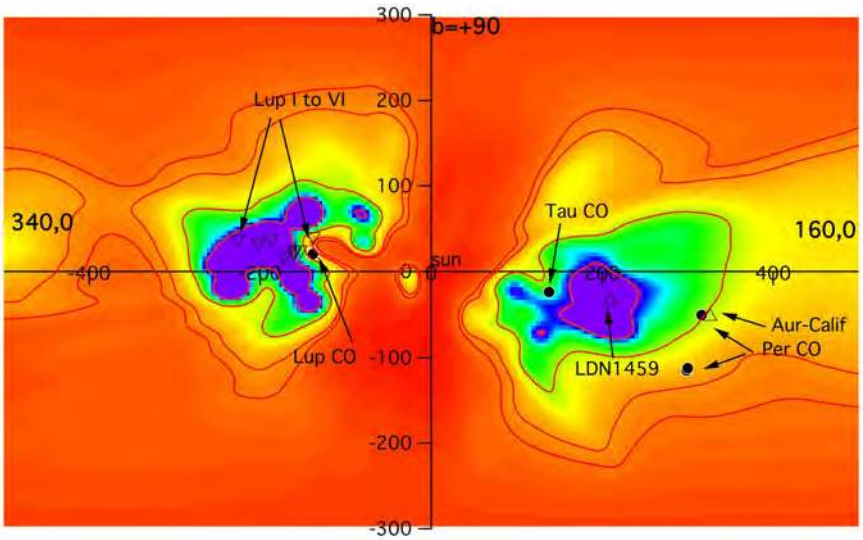

Fig. 10. Same as Fig. 4 for the l = 160–340° plane. Here are shown the locations of the Lupus molecular clouds derived by Knude (2010).

complex at ≃420 pc that appears at a lower latitude on our map. Its distance is in perfect agreement with the 420 pc distance determination of the star EC95 by Dzib et al. (2010), which is also believed to be part of the Serpens cloud. We consider the alignment of the two different clouds as a potential explanation for the discrepancy between the two measurements: the 420 pc cloud may extend at slightly higher latitudes than in our inverted maps, where its northern part is not part of the maps due to the absence of targets stars located beyond the Serpens cloud. Those stars are too extincted. EC95 could be part of it and seen in projection against the Serpens clouds.

There is another potentially interesting feature, this time in the opposite half plane l = 210°. We have drawn in Fig. 4 (bottom) the two directions that mark the limits of thenorthern and southern parts of the Barnard's Loop crescent. Interestingly, they correspond to two elongated parts of a cloud located at ≃170 pc, while the Loop is believed to be associated to the extended Orion region at 440 pc, also visible in the map beyond the 170 pc cloud. We believe that this coincidence deserves further studies of the distance to the Barnard's Loop.

We have also displayed in Fig. 9 the l = 82–262° plane. This specific plane is particular interesting due to the presence of the several objects that gave rise to many discussions and analyses: the Vela supernova remnant (SNR), the Wolf-Rayet system γ_2Vel, the Iras Vela shell (IVS), and the Gum Nebula. In particular, the four were modeled as part of a global scenario by Sushch et al. (2011). The locations of the clouds derived by inversion agree well with this recently devised scenario.

Similarly the l = 160–340° plane drawn in Fig. 10 is particularly rich in clouds. We note here very good agreements between the maps and the cloud distances derived by Knude (2010) for the series of Lupus clouds and LDN1459. The more distant Aur-California dark cloud does not correspond to a very dense region in the map; however, this may be due to the screening effect of Taurus clouds and the lack of targets beyond them.

5. Distance-limited 2D reddening maps

To facilitate the comparison of the inverted 3D distribution with 2D maps based on emission data, we have computed the integral of the differential opacity up to various, selected distances $D_{\rm lim}$ and for one degree steps in longitude and latitude to cover the whole sky. The resulting maps are shown in Figs. 11 and 12. The series of maps at increasing distances from $D_{\rm lim}$ = 100 pc to $D_{\rm lim}$ = 2 kpc allows us to infer at which distances the most conspicuous clouds start to get visible in the 2D maps. In the first and last maps of Fig. 12, which were computed for a radius of 500 pc and 2 kpc resp. We have superimposed the $E(B-V)$ = 0.1 iso-contour of the SFD map. It can be compared with the log $(E(B-V))$ = −1 iso-contour in the 500 pc and

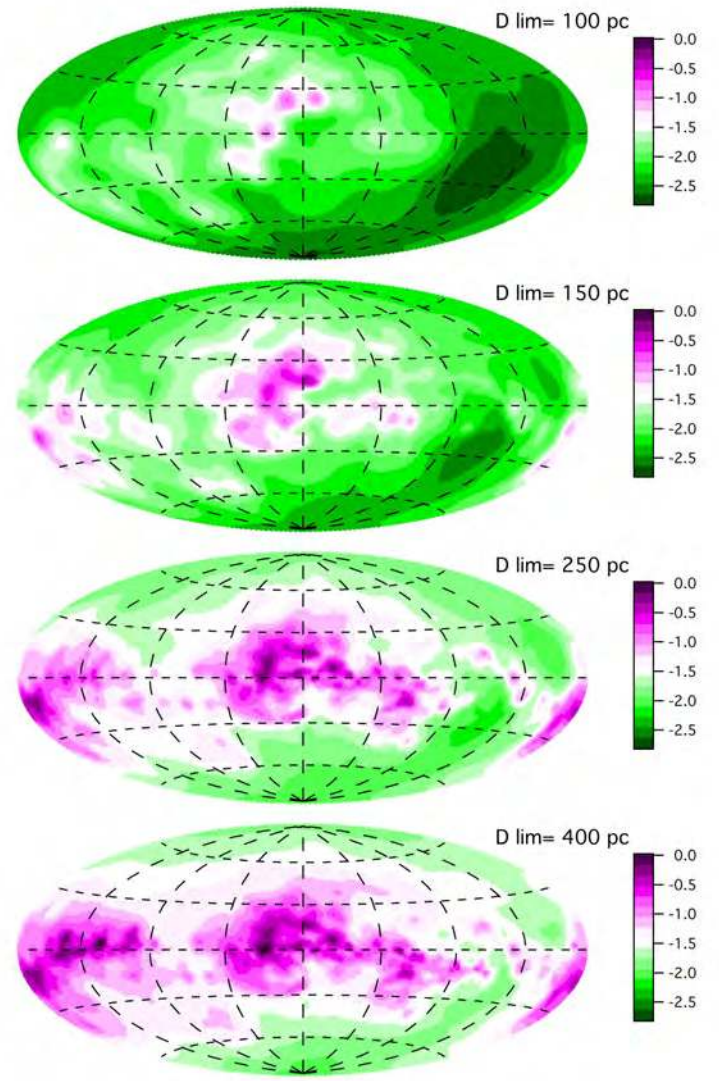

Fig. 11. Opacity $E(B-V)$ from the Sun to the distance $D_{\rm lim}$ = 100, 150, 250, and 400 pc, respectively (*top to bottom*), on a logarithmic scale. The maps are in Aitoff projections, with meridian traces for l = 45, 90, 135, 225, 270, and 315° and parallel traces for b = −60, –30, +30, and +60° shown as dashed and long-dashed lines, resp. The color scale is identical in the four maps.

2 kpc integrated maps (not drawn but easily seen thanks to the white-green transition). Although the inverted maps lack details, the similarities between the two $E(B-V) = 0.1$ contours in the 2 kpc map show that in all directions that define this contour most of the extinction measured by SFD is actually generated closer than 2 kpc and retrieved through the inversion. At variance with the $D_{\rm lim}$ = 2 kpc map, the two contours are significantly different in the $D_{\rm lim}$ = 500 pc map, especially at 90 and 270°. In those directions the extinction is generated beyond 500 pc.

It is important to note that many of the weak features at mid and high latitudes that appear in the vertical planes in Figs. 4 to 7 are not seen in the integrated extinction maps for $D_{\rm lim}$ beyond ≃200–300 pc. This is mainly due to the high differential opacity value chosen for the prior distribution. As a matter of fact, we used a large height scale h_0 = 200 pc, which results in a small decrease of the differential opacity with increasing distance from the plane. This high prior opacity makes the integrated opacity of the tenuous clouds weak or negligible in comparison with the full integrals. However, as we explained above, in practice this large scale height facilitates the detection of the nearby weak features. A typical example of this effect is the case of the North Celestial Pole Loop. The arch that extends from $l \simeq 120°$ to $l \simeq 170°$ and culminates at $b \simeq= 40°$ is clearly seen in the SFD or Planck maps. It appears as a broad extension at high latitude in the $D_{\rm lim}$ = 250 pc map (it is located at ≃200 pc) but does not appear in any of the 2D maps for $D_{\rm lim} \geq 500$ pc. As a conclusion, the search for the distances to the high latitude thin clouds should be essentially performed in the planar cuts in the 3D distribution.

We show in Fig. 13 (resp. Fig. 14) 2D maps of the distance at which the integrated opacity, computed from the inverted differential opacity distribution, reaches the limiting value $E(B-V)$ = 0.02 (resp. 0.06) mag. It allows to visualize where the Local Cavity boundaries are the closest. The closest part of the Aquila Rift and the upper Scorpius and Centaurus regions appear conspicuously. The comparison of those maps as well as Figs. 11 and 12 with the results in distance bins of Reis et al. (2011) show many similarities. More maps of this kind will be presented in a future paper analyzing soft X-ray background data in conjunction with the 3D maps.

6. 3D visualization

The last figure of this article is interactive and represents an iso-differential opacity surface corresponding to 0.0004 mag pc^{-1}, which was made with the YT software (Turk et al. 2011). It allows the global distribution of the main cloud complexes to be visualized. Such a representation, on the other hand, does not allow visualizing details within those surfaces nor visualizing cavity contours. Two additional interactive 3D images showing